LUNDS
UNIVERSITET

Ethylene Oxidation on Palladium Nano Particles Under Temperature Modulations

Noah Preihs

Bachelor's Degree

15 hp at Half-Time 4 month Spring Semester 2026

Supervisor: Jan Knudsen

Co-Supervisor: Ulrike Küst

Division of Synchrotron Radiation at the Department of Physics

Abstract

Ethylene oxidation over Pd nanoparticles in an ambient pressure environment was studied. While modulating the temperature in an ethylene-oxygen mixture, *operando* ambient pressure X-ray photoelectron spectroscopy revealed an oscillating thickness of a PdC_x layer surrounding the nanoparticles while producing CO and CO_2. Scanning electron microscopy before and after the measurement revealed the formation of carbon nanotubes. The carbon nanotubes are likely caused by the removal of carbon from the nanoparticles. The carbon is removed during the cooling half of the temperature cycle.

Keywords

APXPS, Fourier Analysis, Catalysts, Palladium, Nano Particles, Time-Resolved

Table of Contents

Abstract 1
Keywords 1
List of Abbreviations 3
1. Introduction 4
2. Theory 5
2.1. Heterogeneous Catalysis 5
2.2. Ambient Pressure X-ray Photoelectron Spectroscopy 6
2.3. Modulation Excitation Spectroscopy 8
3. Experimental Procedure and Data Processing 10
3.1. Experimental Procedure 10
3.2. Data Processing 10
4. Results and Discussion 10
5. Conclusions and Outlook 15
Acknowledgements 15
Bibliography 15
A. Appendix A: Discussion of $\boldsymbol{O\ 1s}$ and $\boldsymbol{C\ 1s}$ surface spectra 17

List of Abbreviations

XPS	X-ray Photoelectron Spectroscopy
APXPS	Ambient Pressure XPS
MES	Modulation Excitation Spectroscopy
NP	Nano Particle
FA	Fourier Analysis
FT	Fourier Transform
IFT	Inverse FT
S/N	Signal-to-Noise
FE	Fermi Edge
FE calibration spectrum	FE-spectrum
PdC_x	Palladium Carbides
SEM	Scanning Electron Microscopy
CNT	Carbon Nano Tube

1. Introduction

Catalysts are for example used in the exhaust systems of cars, converting toxic molecules as e.g. CO, NO_x and C_xH_y in the exhaust gas to nontoxic ones [1]. The Haber-Bosch process is another prominent example where catalysts are used. In this process, NH_3 is produced from abundant N_2 in the atmosphere [2]. NH_3 is an important chemical for production of fertilisers and many other chemicals. Despite the wide usage of catalysts today, many of them have historically been developed by trial-and-error experiments [3], i.e. different materials and composites have been tested to find the catalyst materials with the best catalytic properties. This method is often time consuming and expensive. If catalyst could be designed from a fundamental understanding of which structures give a certain catalytic function, much could be gained [3].

Industrial catalysts commonly use expensive metals like Pt and Pd as the active catalyst material. For economic reasons, the amount of expensive metal is minimised by producing nanoparticles (NPs) on an inexpensive high-surface-area support material [4]. Therefore, industrial catalyst materials are very inhomogeneous. Additionally, these industrial catalysts are non-conductive, which excludes electron-based characterization techniques due to uncontrolled charging. Both the inhomogeneous samples and the inability to use electron-based techniques results in difficulties to gain a thorough understanding of catalytic processes.

To enable surface science studies with electron-based techniques and to make experiments easier to interpret, it is common to study simplified model systems. Examples of such model systems are polycrystalline foils and single crystal surfaces of the same element(s) or alloy(s) as the active NPs. Both foils and single crystals have a high fraction of bulk atoms. In contrast, NPs have smaller bulk atom fraction but more exposed surface area per atom. A larger bulk volume results in a greater storage capacity of foreign atoms inside the material. Hence, NPs have a considerably smaller storage capacity than foils and single crystals. This possibly alters the electronic structure, resulting in other catalytic properties. Palladium carbide (PdC_x), a material consisting of Pd and C, is one example of a material created by atomic surface deposition – the C atoms deposited on the surface diffuse into the bulk and forms PdC_x.

To study PdC_x formation in NPs, my work focuses on Pd NPs deposited onto a Si wafer substrate that forms a native SiO_2 film. The SiO_2 film is thin enough to be conductive, making electron-based techniques feasible. The choice of PdC_x formation is based on the Pd's wide usage in catalysts, while NPs is chosen to decrease the material gap. Pd is for example frequently used as an active catalyst in the three-way catalyst found in cars, catalysing e.g. the CO oxidation into CO_2 [4]. Because of the many hydrocarbons ($CH_4, C_2H_6, C_2H_4 \dots$) being formed in the engine, Pd is further used since it has been shown to be the metal with the highest CH_4 oxidation rate per unit metal surface [5]. However, if there is insufficient with oxygen, PdC_x can be formed, poisoning the catalyst [4].

The focus of my study is C_2H_4 oxidation. Only one hydrocarbon is used to keep the study simple and easier to interpret. The choice of C_2H_4 comes from its lower oxidation temperature than for example CH_4. This lower oxidation temperature is of importance since previous studies have shown that the Pd NPs can sinter together, i.e. merge, if the temperature is too high [6].

Understanding of carbon formation on the SiO_2 supported NPs under exposure to C_2H_4:O_2-mixtures is found by examining the possible reaction paths. These paths are:

complete oxidation

$$C_2H_4 + 3O_2 \rightarrow 2CO_2 + 2H_2O, \quad (1)$$

partial oxidation

$$C_2H_4 + 2O_2 \rightarrow 2CO + 2H_2O \quad (2)$$

and carbon deposition

$$C_2H_4 + O_2 \rightarrow 2C + 2H_2O. \quad (3)$$

Here, negligible products such as acetaldehyde were excluded. Depending on the amount of oxygen present, each reaction path has a different probability to occur. For Pd polycrystalline surfaces and CH_4 oxidation, it has been shown that CO_2 production dominates when oxygen is abundant and CO production dominates in oxygen lean conditions [7]. Additionally, when all oxygen near the surface is consumed and the so-called oxygen mass transfer limit is reached, carbon deposition via reaction (3) begins to dominate [7, 8].

The surface sensitive Ambient Pressure X-ray Photoelectron Spectroscopy (APXPS) will be used to study the C_2H_4 oxidation, since its time-resolved capabilities are operable during *operando* conditions (whilst the reaction occurs) [9]. Specifically, NPs can be studied while C_2H_4 is oxidised – under *operando* conditions.

Similar to the recent CH_4 oxidation studies [7, 8, 9], which my research is based upon, the temperature will be modulated. Key findings of this study are that it was possible to follow the oxidation reaction of C_2H_4 at operando conditions and that an oscillating carbide formation in response to the temperature modulations was observed.

2. Theory

2.1. Heterogeneous Catalysis

In a heterogeneous catalytic process, the reactants/products are in a different phase than the catalyst material. Since the solid mostly being impenetrable, the catalytic reaction occurs at the surface [4]. The separate phases make the products easily separable from the catalyst, which is of importance to the industry for economic reasons. Otherwise, additional methods would be needed to separate the desired products from the undesired (e.g. the catalyst).

The chemical reaction $X + Y \rightarrow Z$ is shown both with and without the presence of a catalyst in figure 1. For the reaction to occur, the reactants need sufficient energy to overcome the activation barrier E_a [10]. In the presence of a catalyst, the reactants X and Y bind to the catalyst surface. On the catalyst surface, the adsorbed molecules X and Y dissociates and react with a considerably lower E_a than the uncatalyzed reaction (black line in figure 1), forming the product Z. Finally, Z desorbs from the catalyst surface [4]. These steps (adsorption, reaction and desorption), each with their own associated E_a, are the fundamentals of a catalytic reaction. If X or Y are e.g. molecules, then after the adsorption, they would dissociate before reacting and

forming Z [4]. The difference between the energy before the reaction and the largest E_a in one of the catalytic reaction steps (red line in figure 1) is called the apparent E_a ("E_a (with catalyst)" in figure 1).

The catalysed conversion rate K of the reaction $X + Y \rightarrow Z$ is described by the Arrhenius equation

$$K(T) = Ae^{-\frac{E_a}{k_B T}},$$

where A is a pre-factor and k_B is the Boltzmann constant [4]. From the Arrhenius equation, an increase in temperature T, decrease of E_a or a combination leads to an increased conversion rate.

The apparent activation barrier depends on both surface and the reaction pathway; i.e. different surfaces have different apparent activation barriers for different products to be formed (CO_2, CO and C in this study). Therefore, if the Pd NP surface during the *operando* experiments changes, then possibly the catalyst function for the NPs changes and the selectivity towards different reaction products might be altered.

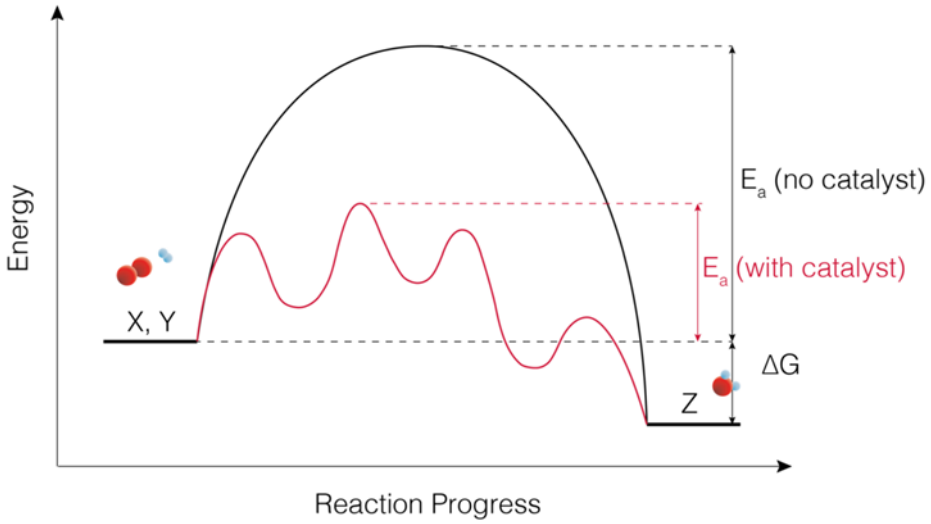

Figure 1: Energy and the activation barrier E_a with (red) and without (black) the presence of a catalyst. ΔG is the total energy change. Taken from [10].

2.2. Ambient Pressure X-ray Photoelectron Spectroscopy

The main principle of X-ray Photoelectron Spectroscopy (XPS) is that a soft X-ray photon with sufficiently high energy $h\nu$ is used to induce electron emission from a surface. By measuring the kinetic energy E_{kin} of the electron and subtracting it from the photon energy, the binding energy of the electron can be found:

$$E_{be} = h\nu - E_{kin}.$$

If E_{be} is defined to be 0 at the Fermi-Edge (FE), it is the energy needed to ionise the core electrons, E_b, combined with the work function Φ. The work function is the minimal energy inducing electron emission from a surface. A change in Φ therefore leads to a change in the measured binding energy. Since Φ is surface dependent, any change of a surface will be seen in the binding energy.

For core electrons, this binding energy E_{be} is unique to every element. For example, the binding energies of $O\ 1s$ and $C\ 1s$ is on the order of 540 eV and 290 eV respectively. However, since different interatomic interactions perturbs the atomic orbitals slightly, the binding energy is also sensitive to the small chemical shifts. From my data in the following analysis, the chemical shift between e.g. CO and CO_2 from $C\ 1s$ is ≈ 2 eV.

Typically, XPS is carried out in ultra-high vacuum for the following reasons: the mean-free-path of photoelectrons is short, the detector has a maximum operating pressure of 10^{-6} mbar and the studied surface needs to be kept clean. However, these conditions do not represent the ones found in real applications of catalysis that often takes place in high pressures and temperatures. A pressure gap between industrial applications and experiments exists.

To overcome this pressure gap and approach real applications, *operando* studies (while the reaction occurs) in ambient gas pressures are common. However, increasing the gas pressure results in shorter mean-free-paths of the photoelectrons.

One approach to overcome the short mean-free-path is to position a nozzle (A, figure 4) close to the sample. As a rule of thumb, the separation between the sample and nozzle should be twice the nozzle diameter: for a diameter of 300 µm, the separation should be 600 µm. The small separation results in short electron travel paths in pressurised gas. In the differential pumping stages (B – D, figure 4), the pressure at the nozzle is reduced to 10^{-6} mbar in the hemispherical analyser. This combination is used to enhance the number of collected electrons in ambient pressure (AP) XPS measurements, which increases the signal strength [15].

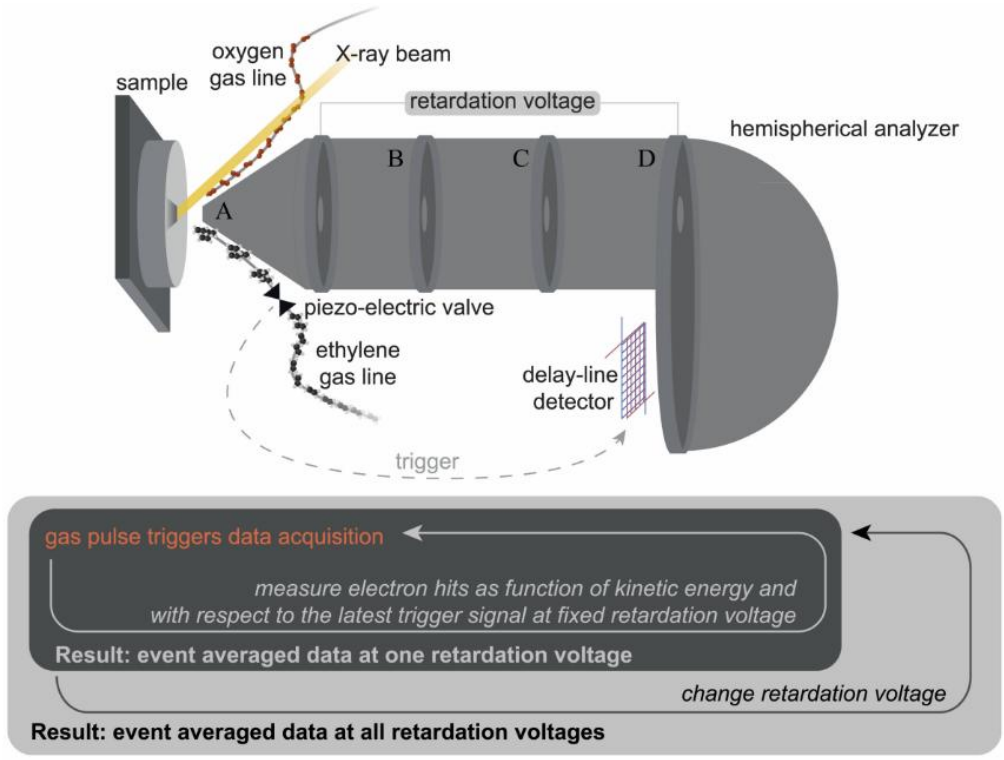

Figure 2: Schematical view of the set up. The nozzle (A) collects the electrons, which are transported through several differential pumping stages (B – D) to the hemispherical analyser. The pressure in A is reduced through B – D before the analyser. Taken from [1].

For my experiments, the AP cell at the APXPS endstation of the SPECIES beamline at MAX IV Laboratory in Lund was used. In this cell, the upper pressure and temperature limits are 20 mbar and 600°C. The cell volume of ≈ 200 ml [16] makes it possible to swiftly exchange the gas composition, enabling experiments with periodic variations in gas compositions over time [17]. Coupled to the inlet and outlet flows of the AP chamber is a Quadrupole Mass Spectrometer, enabling a measuring of products and reactants simultaneously as the XPS spectra are acquired [18].

2.3. Modulation Excitation Spectroscopy

Studies of catalysts that either change structure or composition dynamically during static or changed reaction environment conditions, belongs to the category of dynamic catalysis studies. Such studies have increased over the proceeding years. One major reason is that often the active surfaces of the catalysts undergo dynamical changes over time [9], such as structural changes [11], which static parameters cannot depict clearly [9]. Another reason to focus on dynamical properties is that actively participating and spectator species can be distinguished [12]. Hence, the concepts of Modulation Excitation Spectroscopy (MES) can be used for these time-resolved studies. The fundamental principle relies on one or several variable(s) being modulated while another, possibly depending, response is being measured. Figure 2 depicts the modulated signal $I_m(t)$ and how the resulting modulations of e.g. the spectrum $I(t)$ responds [9].

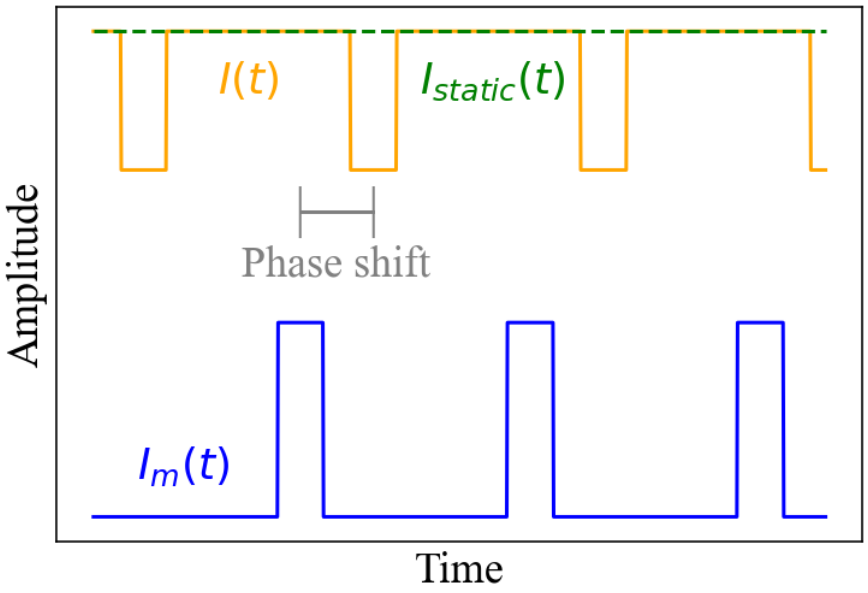

Figure 3: Excitation Modulation Spectroscopy schematically shown. The modulated intensity $I_m(t)$ affects the response signal $I(t)$, possibly with a phase shift. The image is inspired by [9].

The modulated signal $I_m(t)$ can e.g. be the temperature and the response signal $I(t)$ the intensity from a gaseous environment, delayed from $I_m(t)$ [7, 9]. APXPS is one example where MES can be applied [13].

In this context, the group of J. Knudsen has developed a Fourier Analysis (FA) methodology enabling quick time-resolved signal processing [9]. For a typical APXPS spectrum, the intensity $I(E,t)$ is measured as a function of binding energy and time. By choosing a specific binding energy, it is possible to study a signal that only depends on time: $I(E,t) \rightarrow I(t)$. Since the intensity at a given binding energy is only time dependent, it is possible to apply the algorithms of Fourier Transform (FT) on $I(t)$, transforming it from the real time space to the complex

frequency space $\tilde{I}(f)$ [13]. Panel A in figure 3 depicts an oscillating signal (in red) and panel B the resulting complex frequency space, which is the result of a FT (arrow 1).

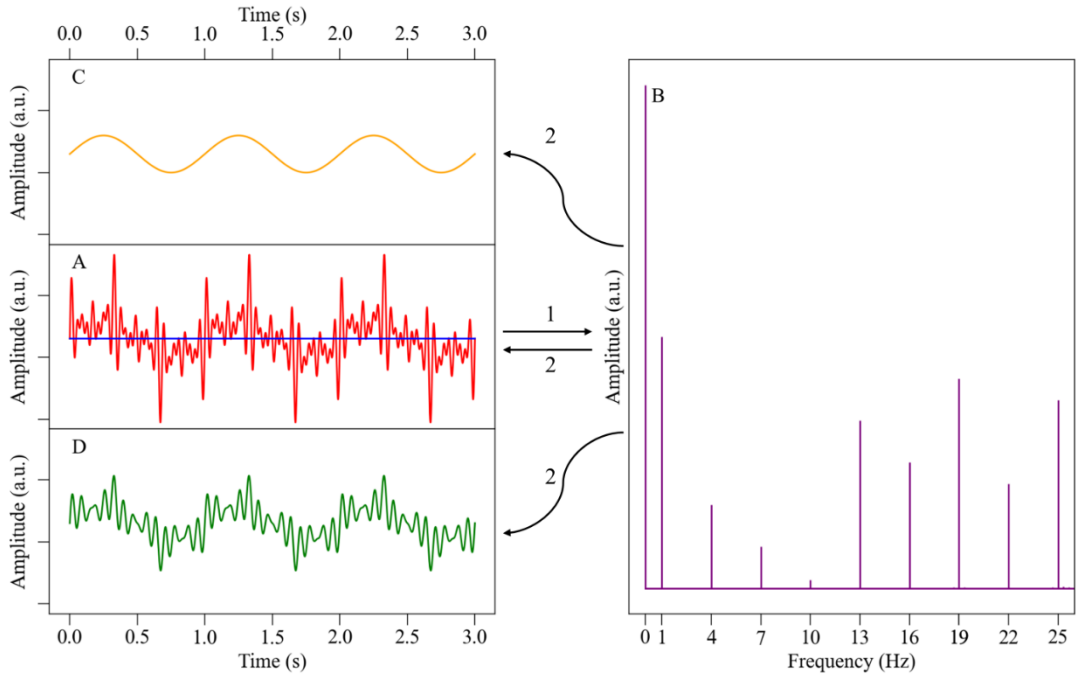

Figure 4: Schematical overview of FT – inverse FT. The red signal in (A) is being (1): FT to (B) and (2): inverse FT with (C): 0 overtones and (D): 6 overtones. The blue signal in (A) is the static background.

In the complex frequency space, each coordinate $\left(f, \tilde{I}(f)\right)$ can be expressed in polar coordinates $\big(A(f), \phi(f)\big)$, where A is the amplitude and ϕ is the phase [9]. This reasoning can be extended for any binding energy, making A and ϕ dependent on both binding energy and frequency: $A(E, f)$ and $\phi(E, f)$ [13].

A periodic signal (see the red graph in panel A) will be able to be written as a sum of sines [14] with different frequencies, i.e. overtones (see panel B) [9]. Therefore, $I(E, t)$ can be written as

$$I(E,t) = \sum_f A(E,f) \cdot \sin\big(2\pi f t + \Phi(E,f)\big).$$

The more overtones considered, the more exact the periodic behaviour of the catalytic activity will be depicted. Panel C and D show the inversed FT signal (arrow 2) when including the zeroth and 6 first overtones, respectively. However, the signal-to-noise (S/N) ratio will decrease when increasing the number of included harmonics. This means that a weighting between depicting the oscillatory behaviour and increasing the S/N-ratio, when performing the inverse FT (IFT), is needed [9].

Moreover, including the $f = 0$ Hz frequency when performing the IFT will include the static background [13], depicted as the blue line in panel A. Neglecting the $f = 0$ Hz frequency (the static background) will showcase only the intensity variations. As discussed in [13], undetectable oscillatory signals in the raw data can easily be detected in the frequency space after a FT.

3. Experimental Procedure and Data Processing

3.1. Experimental Procedure

Pd NPs covering 10% of the sample surface were studied. A silicon wafer was used as support for the NPs. $C\ 1s$, $O\ 1s$, $Pd\ 3d$ and $Si\ 2p$ core levels were probed with a photon energy of 800 eV, 1050 eV, 850 eV and 614 eV, respectively. $C\ 1s$ and $O\ 1s$ spectra were measured with the sample in the normal XPS position and with it retracted by 300 µm. Hereby, the sample was positioned in a surface sensitive and gas sensitive position respectively. Pd and Si were only studied with the sample in the surface position. For all spectra, 10 000 scans were acquired, with an acquisition frequency of 8 Hz. For each surface spectrum, a FE calibration spectrum (FE-spectrum) was taken with the same photon energy. FE-spectra were only scanned once.

When mounted in the AP cell, the sample was irradiated with an infrared laser from behind, leading to sample temperature oscillations between 450°C and 550°C. The temperature was changed at a constant rate of 2.5°C/s, both when increasing and decreasing. Meanwhile, a gas flow of 0.5 sccm: 1 sccm O_2: C_2H_4 was maintained with mass flow controllers at a constant 1 mbar pressure.

3.2. Data Processing

The raw-data was calibrated to the FE, followed by a normalisation of the time-resolved $O\ 1s$ surface, $C\ 1s$ surface, $Pd\ 3d$ and $Si\ 2p$ spectra. Normalisation was performed on these spectra, to account for the changing gas composition in-between the nozzle and surface. Hence, the mean-free-path of the electrons changes, resulting in a changing photoelectron transmission resulting in a varying background. Conversely, the gas-phases time-resolved spectra are not normalised, since the change of the gases are of interest. After the normalisation, the FT was applied to each time-resolved spectrum, followed by an IFT. After the IFT, the time was calibrated to align the temperature cycles.

A polynomial background was fitted and subtracted from each spectrum, i.e. the spectrum at each time measurement. Since the time-resolved spectrum was varying smoothly over time, a binning of 5 was used to enhance the S/N-ratio.

The energy resolution of the photon and electron analyser gives a Gaussian distribution. Moreover, the lifetime of the core hole gives a Lorentz distribution. The analytical approximated convolution of these two distributions is called a pseudo-Voigt distribution. The peaks were fitted with a Pseudo-Voigt-profile on the average of all the spectra of the time-resolved spectrum. This was done to determine the width, binding energy and Gaussian-Lorentzian-ratio, which later were fixed to these fitted values. Then, from curve fits on each peak in each spectrum, the intensities as functions of time were extrapolated. The specimen each peak belonged to were determined with the help of literature.

4. Results and Discussion

The gas phase's response to the temperature modulations is depicted in figure 5. The temperature oscillations are seen in panel G. In panel A and D, image plots of $O\ 1s$ and $C\ 1s$ spectra are shown. Selected spectra and their curve fits at high (t_{Thigh}) and low (t_{Tlow}) temperatures are shown in panel B, C and E, F respectively.

In the $O\ 1s$ gas phase one can observe O_2, CO, CO_2 and H_2O from left to right [1, 7, 8], while in the $C\ 1s$ gas phase, C_2H_4 shake-up, CO_2, CO and C_2H_4 are observed [1]. Additionally, an undetermined peak (marked with ?) is present to the far left.

Because of the low signal amplitude of the CO and CO_2-peaks in the $O\ 1s$ time-resolved gas phase spectrum, their binding energy position and widths were based on the more intense O_2 peak. This was possible since the binding energy difference between O_2 and CO/ CO_2 is known.

By comparing the $O\ 1s$ and $C\ 1s$ spectra at t_{Tlow} and t_{Thigh} in panel C, B and F, E, O_2, CO_2, C_2H_4 and its shake-up are observed to be present at both temperatures. The fact that CO_2 is present is clear evidence for the catalyst being active.

In contrast to the other reaction products, CO is only observed at t_{Thigh}. This is evident by looking at the $C\ 1s$ spectrum (panel E and F). The CO in the $O\ 1s$ spectrum overlaps largely with the broad O_2 peak (see panel C) and it is therefore not evident that CO is observed only at t_{Tlow}. Hence, the discussion of CO will be based on its evolution in the $C\ 1s$ spectrum.

Opposite, the undetermined peak, the C_2H_4 shake-up and CO_2-peak in the $C\ 1s$ spectrum are difficult to perform a background subtraction on. Hence, these are not quantifiable and will be disregarded in the further analysis. Instead, CO_2 is better determined from the $O\ 1s$ gas phase spectrum; therefore, the discussion of CO_2 will be based on its evolution in the $O\ 1s$ spectrum.

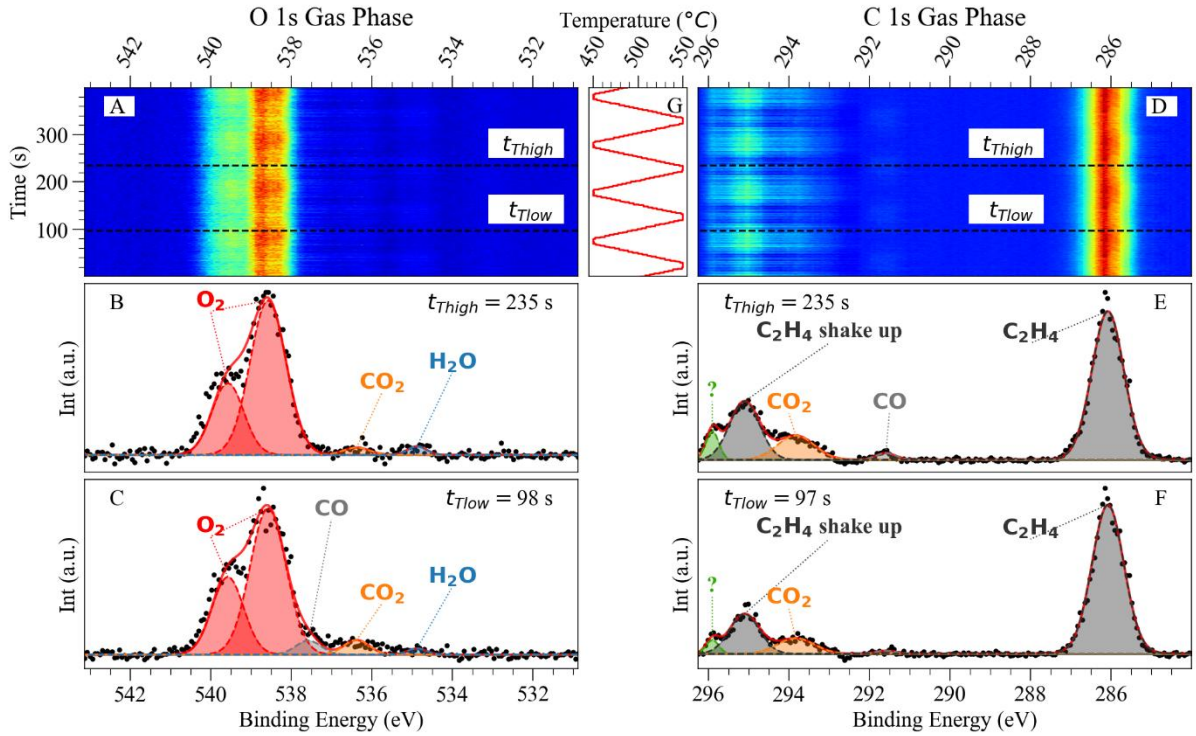

Figure 5: (A) Image plot of $O\ 1s$ gas phase spectra. (B)/(C) Selected spectrum for $O\ 1s$ with curve fits at t_{Thigh}/t_{Tlow}. (D) Image plot of $C\ 1s$ gas phase spectra. (E)/(F) Selected spectrum for $C\ 1s$ with curve fits at t_{Thigh}/t_{Tlow}. (G) The temperature oscillation as a function of time. The temperature increases to the right.

Understanding of the gas phase response to the modulated temperature requires a study of the surface, which will be the focus of the following discussion. $Pd\ 3d$ and $Si\ 2p$ spectra, displayed in figure 6, will be analysed. Figure 6 has a similar layout as figure 5.

From the left to the right, PdC_x and Pd_{bulk} are visible in the $Pd\ 3d$ spectrum (panel B) [7]. Further evidence for the assignment of the PdC_x component can be found in the $C\ 1s$ surface spectrum with the corresponding discussion in appendix A. In the $Si\ 2p$ spectrum, SiO_2 and Si are observable (panel E).

An important observation is the change in relative intensity between PdC_x and Pd_{bulk} at the different temperatures (see panel B and C and the shoulder marked with a black circle to the right in panel A). This indicates a compositional change of the NP surface throughout the temperature cycle. In contrast, the Si components display no significant changes.

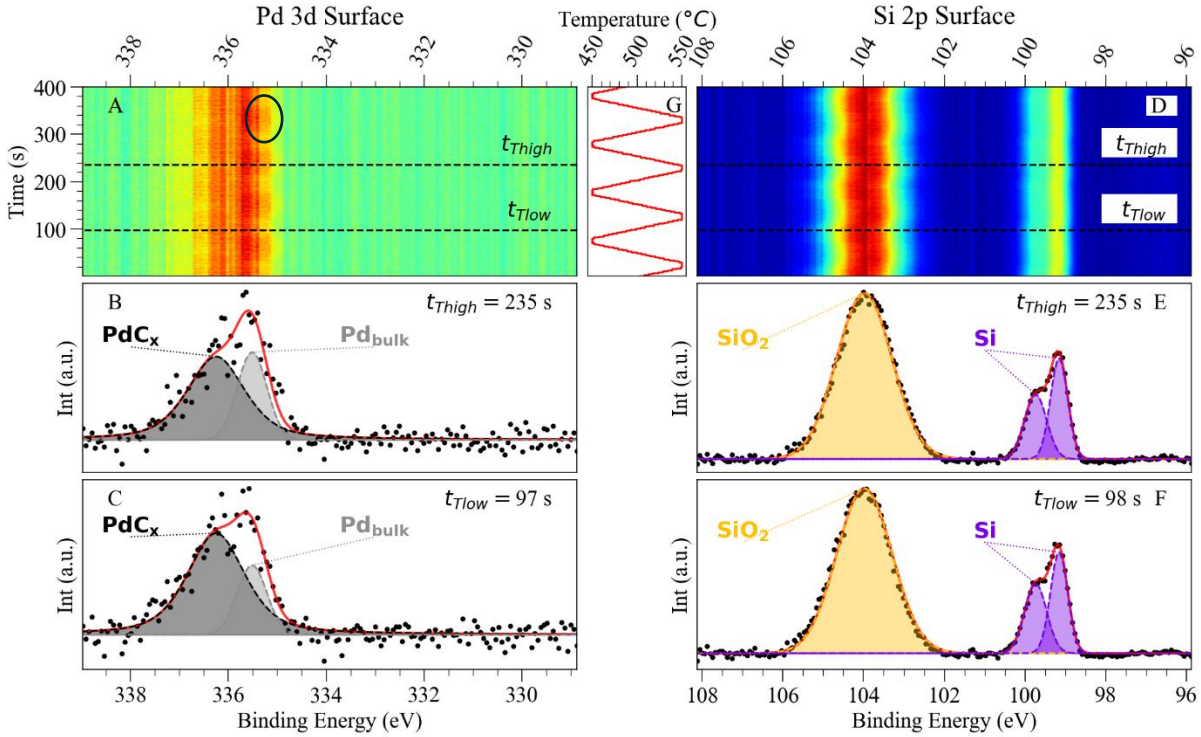

Figure 6: (A) Image plot of Pd 3d gas phase spectra. (B)/(C) Selected spectrum for Pd 3d with curve fits at t_{Thigh}/t_{Tlow}. (D) Image plot of Si 2p gas phase spectra. (E)/(F) Selected spectrum for Si 2p with curve fits at t_{Thigh}/t_{Tlow}. (G) The temperature oscillation as a function of time. The temperature increases to the right.

Curve-fitting all spectra in the same way as shown in figure 5 and 6, panel B, C, E and F, the gas phase and surface response to the modulated temperature can be studied in detail. The spectrum characteristic peak intensity is related to the species concentration when it is the only free fitting parameter. Therefore, the fitted peak intensities represent the species concentrations response to the modulated temperature.

The gas phase and surface specimen spectrum intensities (panel A and C respectively) is plotted with the modulated temperature (panel B) in figure 7. Some species intensities (marked with a multiplication sign) were scaled for better visibility, and all intensities were smoothed (the lines in figure 7).

In panel A, the intensity from O_2 and C_2H_4 decreases when the temperature increases, while the reaction products CO, CO_2 and H_2O intensities increase. This is clear evidence that this study has been able to follow the catalytic response to the temperature.

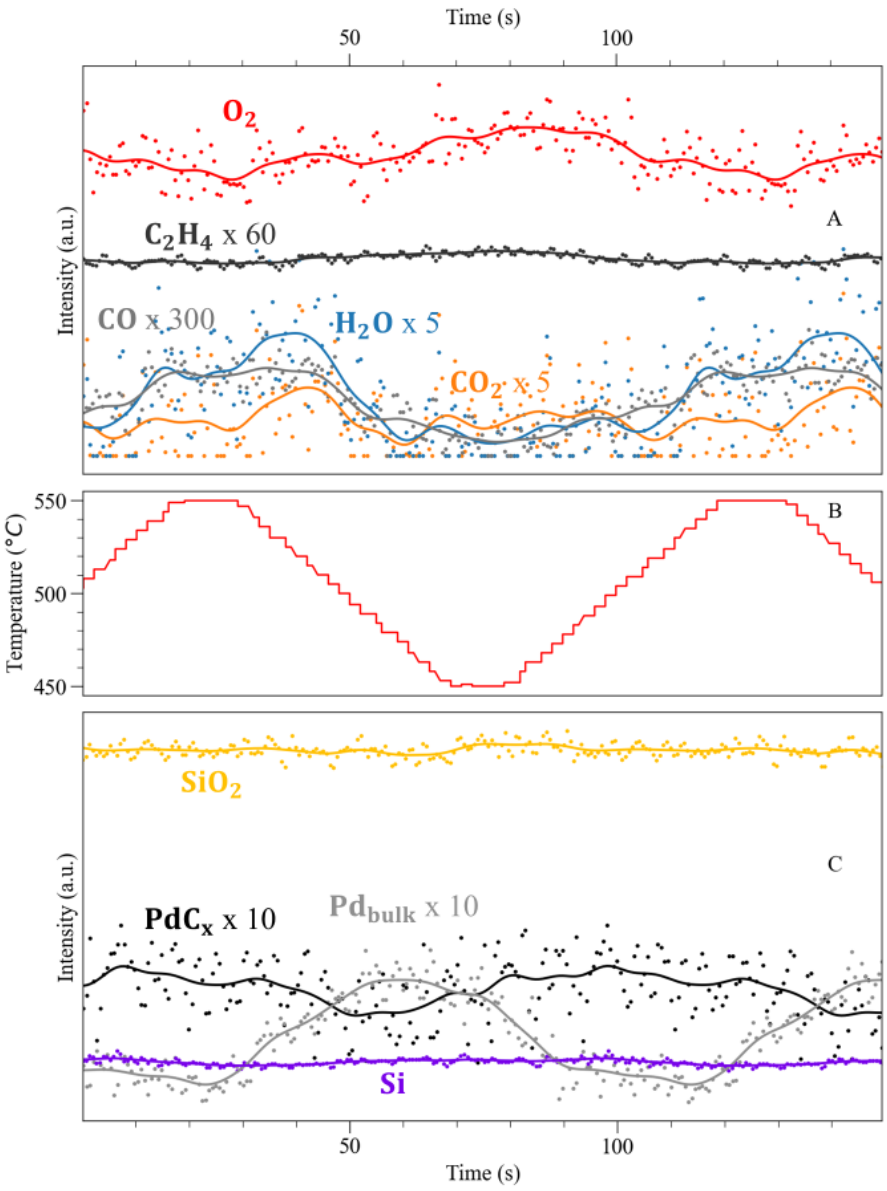

Figure 7: The fitted intensities as a function of time. (A) The gas phase. (B) The modulated temperature. (C) The surface of Pd and Si.

A key observation is the alternating strength between PdC_x and Pd_{bulk} in panel C, figure 7, which suggests an alternating thickness of a PdC_x layer surrounding the NPs. Figure 8 depicts this schematically; when the temperature increases (decreases), the black PdC_x layer grows thicker (thinner). The Pd species strength alternation correlates with the temperature. When increasing the temperature, PdC_x (Pd_{bulk}) is observed to increase (decrease). In parallel, the formation of CO, CO_2 and H_2O is increased (panel A and B) – main evidence for an oxidation reaction. C depositing on the NP surfaces (oxidation reaction (3)) is strongly supported by the occurrence of the oxidation products and PdC_x – diffusing into the NPs, C reacts with Pd and forms PdC_x. The PdC_x layer is most reasonable to be at the surface of the NPs, since this is where the C is deposited. The supporting Si wafer depicts no clear oscillations with the modulated temperature. Notably, it appears that Si is a spectator species in the reactions.

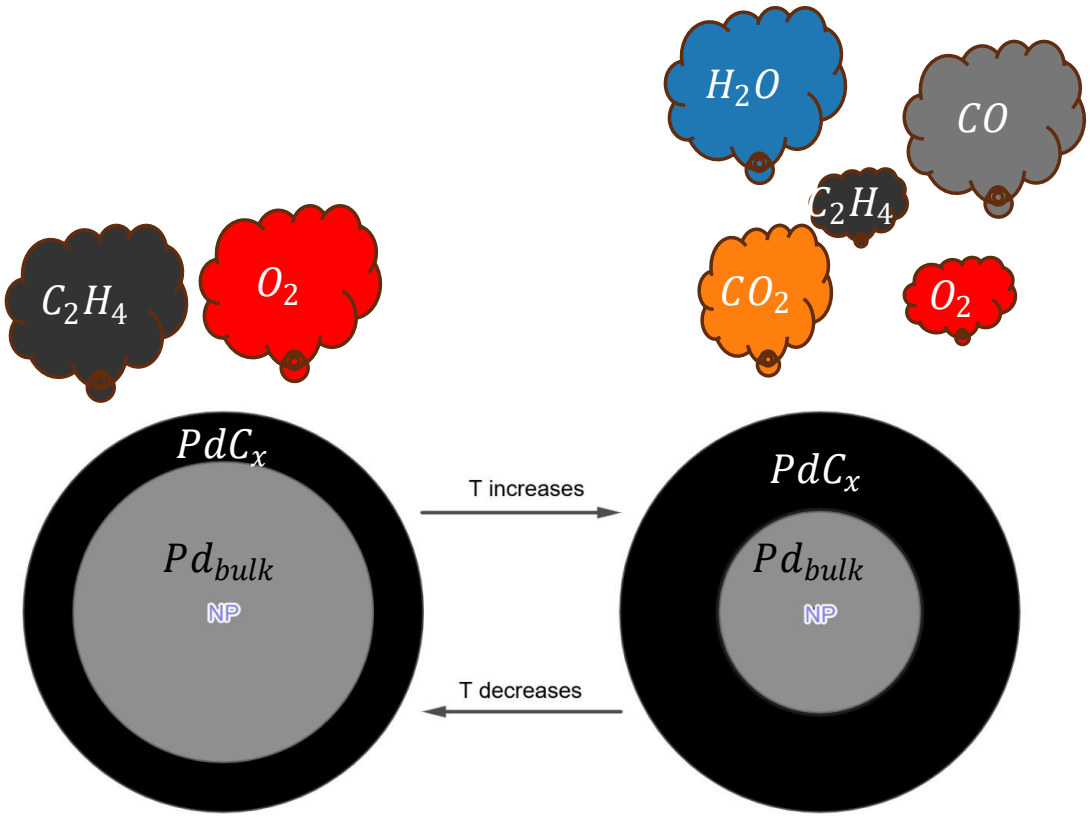

Figure 8: A schematical overview of the changes of the surface structure over the NPs depending on the temperature.

In addition to the APXPS measurements, two Scanning Electron Microscopy (SEM) pictures of the sample were taken (figure 9): one before and one after the experiment. In figure 9 before the experiment, the white NPs are distinguishable from each other and the SiO_2 support. A minor fraction of the NPs is observed to have sintered together. After the measurement, some NPs are visible as bright dots; notably, tubular structures are present.

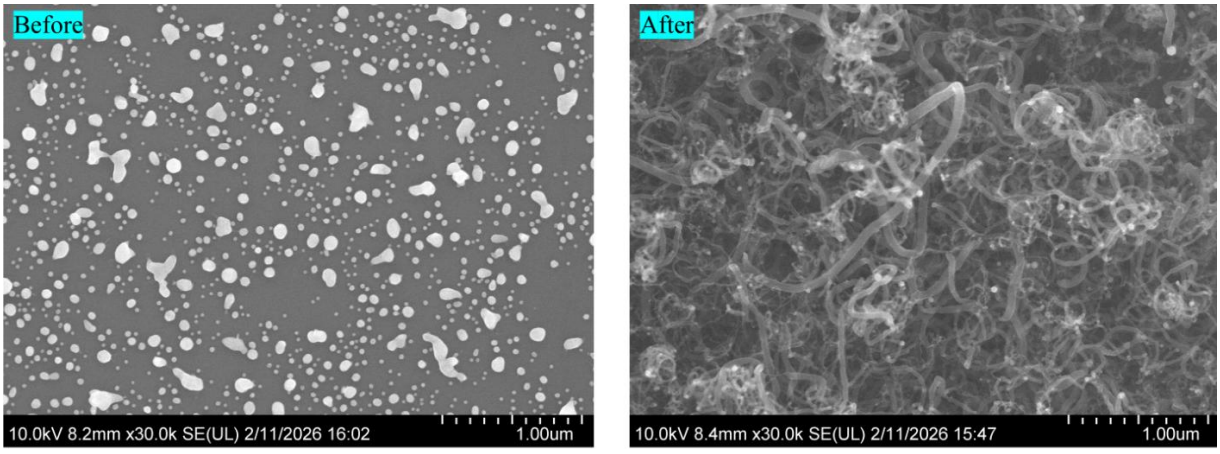

Figure 9: NPs (white dots) on a SiO_2 support before and after the experiment.

The tubes formed on the catalyst's surface are most probably assigned as multiwalled carbon nano tubes (CNT), with Pd/PdC_x NPs at the end. As the deposited carbon is removed from the NPs, it is in the form of CO, CO_2 and CNTs. This enables new carbon to be deposited at the surface, forming PdC_x and repeating the process. The carbon not removed in the form of CO and CO_2 are instead building the CNTs, pushing them from the NPs and creates complex

structures [19, 20]. The PdC_x response from the temperature modulations in figure 7 clearly induces the CO_2 production. However, with the important discovery of CNTs, an oscillating CNT growth is possibly induced when modulating the temperature. The uncontrolled growth of these CNTs might eventually cover the active NPs, preventing the catalytic activity [21].

5. Conclusions and Outlook

In this study, Pd NPs supported on a SiO_2 wafer was exposed to a C_2H_4: O_2 gas mixture in the mbar regime at constant pressure while modulating the temperature. The surface and the gas nearby were characterised with the APXPS, improved by Fourier transformation methodology developed in the group of J. Knudsen.

At the highest temperatures during the temperature modulations, C_2H_4 were oxidised into both CO and CO_2. Meanwhile, PdC_x was formed on the surface of the Pd NPs. Opposite, at the lowest temperature of modulation, an increased Pd_{bulk} signal and a weak oxidation was observed. The SiO_2 support did not respond to the temperature modulation. SEM images recorded after the APXPS measurements revealed that the sample was covered in a tube-like pattern, possibly stemming from the formation of carbon nanotubes growing out from the PdC_x covered nano particles.

To study C_2H_4 oxidation in lean conditions catalysed by the Pd nano particle with an environmental transmission electron microscopy would be a very interesting follow-up study. Such a study might show the dynamics of the CNT formation, and it might even be possible to link this to the oscillating PdC_x formation.

Acknowledgements

I would like to thank my supervisor Jan Knudsen and co-supervisor Ulrike Küst for helping and allowing me to do this project. Thanks for answering my questions and helping me think in new ways. I would also like to thank the SPECIES beamline staff for helping the experiment run smoothly and thanks to Hajar Jalili and Rasmus Westerström for producing the nanoparticles for the experiment. And thanks to my mother and family for supporting me through this project and proofreading my text.

I would also like to take the opportunity to give notice of the usage of Microsoft Copilot – a tool experimented with for sentence structure. Copilot was asked how a sentence could be improved based on formal, academic English writing. From the suggested sentence structure, some wording was changed in the text, but some of Copilots suggestions were disregarded as they would not fit my language of writing.

Bibliography

[1] U. Küst, C. Eads, J. Prumbs, W. Wang, R. Temperton, A. Klyushin, A. Shavorskiy and J. Knudsen, ”Operando hysteresis of a palladium surface during high-frequency gas-pulsing of ethylene into oxygen,” *Surface Science,* vol. 766, 2026.

[2] ”Fritz Haber – Facts,” Nobel Prize Outreach 2026, [Online]. Available: https://www.nobelprize.org/prizes/chemistry/1918/haber/facts/. [Used 11 March 2026].

[3] M. Campanati, G. Fornasari and A. Vaccari, ”Fundamentals in the preparation of heterogeneous catalysts,” *Catalysis Today,* vol. 77, nr 4, pp. 299-314, 2003.

[4] I. Chorkendorff and J. W. Niemantsverdriet, Concepts of Modern Catalysis and Kinetics, Weinheim: Wiley-VCH Verlag GmbH & Co. KGaA, 2003.

[5] D. Zemlyanov, B. Aszalos-Kiss, E. Kleimenov, D. Teschner, S. Zafeiratos, M. Hävecker, A. Knop-Gericke, R. Schlögl, H. Gabasch, W. Unterberger, K. Hayek and B. Klötzer, ”In situ XPS study of Pd(111) oxidation. Part 1: 2D oxide fomration in 10-3 mbar O2,” *Surface Science,* vol. 600, pp. 983-994, 2006.

[6] H. A. Khan, J. Hao, O. E. Tall and A. Farooq, ”Yttrium stabilization and Pt addition to Pd/ZrO2 catalyst for the oxidation of methane in the presence of ethylene and water,” *RSC Advances,* vol. 11, pp. 11910-11917, 2021.

[7] U. Küst, W. Wang, C. Wang, H. Hagelin-Weaver, J. Gustafson, A. Shavorskiy, J. F. Weaver and J. Knudsen, ”Temperature-Dependent Selectivity and Detection of Hidden Carbon Deposition in Methane Oxidation,” *ACS Publications,* vol. 14(8), pp. 5978-5986, 2024.

[8] U. Küst, R. Jones, J. Prumbs, A. Namar, M. Scardamaglia, A. Shavorskiy and J. Knudsen, ”Carbon subsurface traffic jam as driver for methane oxidation activity and selectivity on palladium surfaces,” *Nature Communications,* vol. 16, 20 August 2025.

[9] U. Küst, J. Prumbs, C. Eads, W. Wang, V. Boix, A. Klyushin, M. Scardamaglia, R. Temperton, A. Shavorskiy and J. Knudsen, ”Comparing phase sensitive detection and Fourier analysis of modulation excitation spectroscopy data exemplified by Ambient Pressure X-ray Photoelectron Spectroscopy,” *Elsevier,* vol. 751, January 2025.

[10] V. Boix de la Cruz, ”Graphene: Applications in Surface Science Studies,” Media-Tryck, Lund, 2022.

[11] S. Chavez, B. Werghi, K. M. Sanroman Gutierrez, R. Chen, S. Lall and M. Cargnello, ”Studying, Promoting, Exploiting, and Predicting Catalyst Dynamics: the Next Frontier in Heterogeneous Catalysis,” *The Journal of Physical Chemistry,* vol. 127, nr 5, pp. 2127-2146, 2023.

[12] A. Urakawa, D. Ferri and R. J. G. Nuguid, ”Modulation Excitation Spectroscopy (MES),” *Springer Handbook of Advanced Catalyst Characterization,* pp. 967-977, 18 May 2023.

[13] J. Knudsen, C. Eads, A. Klyushin, R. Temperton, U. Küst, V. Boix, A. Kraina, M. Scardamaglia, A. Shavorskiy, E. Kokkonen and J. Schnadt, ”Catalysis in Frequency Space: Resolving Hidden Oscillating Minority Phases and Their Catalytic Properties,” *ACS Publications,* vol. 15, pp. 1655-1662, 2025.

[14] A. Wacker, Compendium Mathmatical Methods for Vibrations, Waves and Diffusion, Lund: Andreas Wacker, 2024.

[15] N. Johansson, Synchrotron-based In Situ Electron Spectroscopy Applied to Oxide Formation and Catalysis, Lund, Skåne: Media-Tryck, 2017.

[16] E. Kokkonen, F. Lopes da Silva, M.-H. Mikkelä, N. Johansson, S.-W. Huang, J.-M. Lee, M. Andersson, A. Bartalesi, B. N. Reinecke, K. Handrup, H. Tarawneh, R. Sankari, J. Knudsen, J. Schnadt, C. Såthe and S. Urpelainen, ”Upgrade of the SPECIES beamline at the MAX IV Laboratory,” *Journal of Synchrotron Radiation,* vol. 28, pp. 588-601, 2021.

[17] J. Knudsen, J. N. Andersen and J. Schnadt, ”A versatile instrument for ambient pressure x-ray photoelectron spectroscopy: The Lund cell approach,” *Elsevier,* vol. Surface Sceince 646, pp. 160-169, 2016.

[18] S. Urpelainen, C. Såthe, W. Grizolli, M. Agåker, A. R. Head, M. Andersson, S.-W. Huang, B. N. Jensen, E. Wallén, H. Tarawneh, R. Sankari, R. Nyholm, M. Lindberg, P. Sjöblom, N. Johansson, B. N. Reinecke, M. A. Arman, L. R. Merte, J. Knudsen, J.

Schnadt, J. N. Andersen and F. Hennies, ”The SPECIES beamline at the MAX IV Laboratory: a facility for soft X-ray RIXS and APXPS,” *Journal of Synchrotron Radiation,* vol. 24, pp. 344-353, 2017.

[19] S. Helveg, J. Sehested and J. R. Rostrup-Nielsen, ”Whisker carbon in perspective,” *Catalysis Today,* vol. 178, nr 1, pp. 42-46, 15 December 2011.

[20] M. A. Atwater, J. Phillips, S. K. Doorn, C. C. Luhrs, Y. Fernández, J. A. Menéndez and Z. C. Leseman, ”The production of carbon nanofibers and thin films on palladium catalysts from ethylene–oxygen mixtures,” *Carbon,* vol. 47, nr 9, pp. 2269-2280, August 2009.

[21] R. Waelder, C. Park, A. Sloan, J. Carpena-Núñez, J. Yoho, S. Gorsse, R. Rao and B. Maruyama, ”Improved understanding of carbon nanotube growth via autonomous jump regressions targeting of catalyst activity,” *Carbon,* vol. 228, 2024.

[22] V. R. Fernandes, M. Van den Bossche, J. Knudsen, M. H. Farstad, J. Gustafson, H. J. Venvik, H. Grönbeck and A. Borg, ”Reversed Hysteresis during CO Oxidation over $Pd_{75}Ag_{25}$(100),” *ACS Catalysis,* vol. 6, pp. 4145-4161, 2016.

A. Appendix A: Discussion of O 1s and C 1s surface spectra

The time averaged surface spectra of O 1s and C 1s are depicted in panel A and B, figure 10 below, respectively. Two undefined, curve-fitted peaks in panel A are found to the far left. Pd 3p is present between approximately 528.5 eV and 529 eV [1, 22]. In panel B, a curve-fitted C_2H_4 peak is present [1].

The information in the Pd 3p peak can be found in the Pd 3d peak in figure 6, i.e. Pd_{bulk} and PdC_x. However, one cannot reliably distinguish the different Pd-peaks due to the small intensity in Pd 3p. Therefore, it is not included in the analysis.

Apart from the strong C_2H_4 peak in panel B, there is a peak between approximately 284 eV and 285 eV. Between these binding energies, there is an intensity greater than the curve fit belonging to PdC_x [1]. This fortifies the claim of seeing PdC_x for Pd 3d in figure 6.

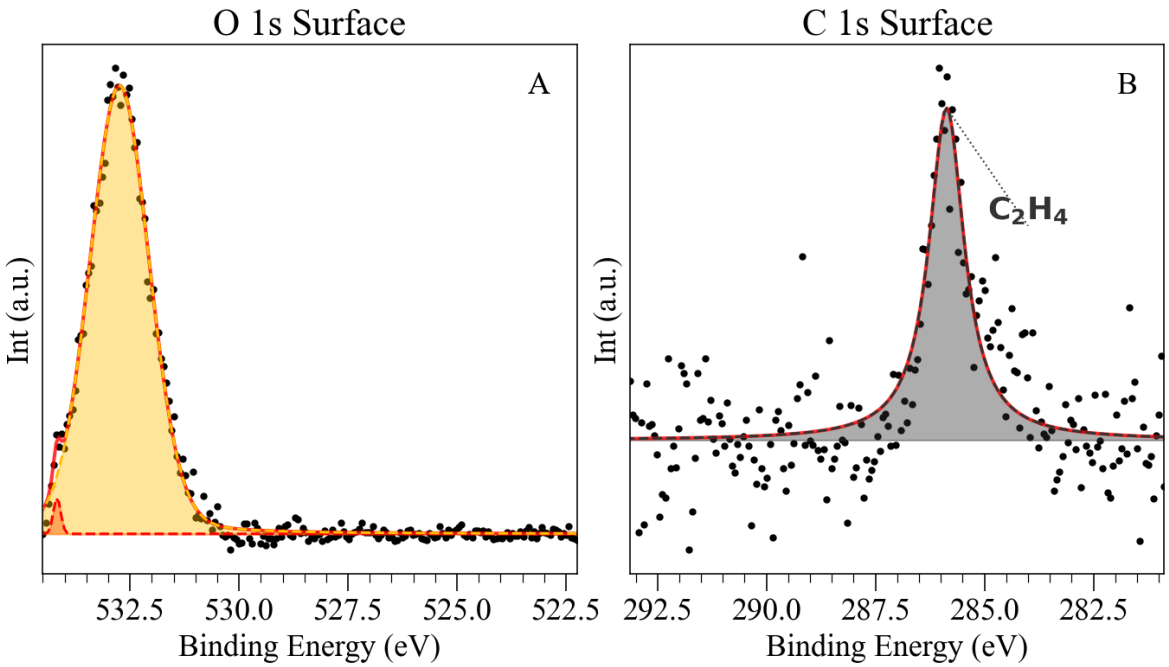

Figure 10: The average spectrum over time for (A) O $1s$ and (B) C $1s$. (A) Pd $3p$ is present between binding energies 528.5 eV and 529 eV. Pd $3p$ have not been fitted with a curve. (B) A C_2H_4 peak (fitted with a curve) and a PdC_x peak.